Available online at www.sciencedirect.com
SCIENCE DIRECT®
International Journal of Industrial Ergonomics 34 (2004) 375–394
International Journal of Industrial Ergonomics
www.elsevier.com/locate/ergon

A mathematical method for ergonomic-based design: placement

Karim Abdel-Malek[a,*], Wei Yu[a], Jingzhou Yang[a], Kyle Nebel[b]

[a] *Virtual Soldier Research Program, Department of Mechanical Engineering and Center for Computer-Aided Design, The University of Iowa, 116 Engineering Research Facility, Iowa City, IA 52242-1000, USA*
[b] *U.S. Army TACOM/RDECOM, AMSRD-TAR-NAC/157, 6501 East 11 Mile Rd., Warren, MI 48397-5000, USA*

Available online 7 July 2004

Abstract

A rigorous mathematical formulation for ergonomic design based on obtaining and visualizing the workspace of human limbs is herein presented. The methodology and formulation presented in this paper are aimed at placing the human with respect to specified targets, whereby optimizing a given human performance measure. These measures are developed as mathematical cost functions that can be maximized or minimized. For example, as a result of this analysis, a method for placing the human operator relative to the controls in an assembly line while minimizing the person's stress at each joint can be achieved. Other cost functions such as maximizing reachability or maximizing dexterity are considered. The method is characterized by two steps: (1) determine the boundary envelope (also called reach envelope) of a human limb in closed form as, and, (2) move the workspace envelope towards optimizing the cost function while satisfying all constraints. By defining a new position and orientation of the limb's workspace with respect to the target points, it is possible to establish an ergonomic design that satisfies the given constraints. The strengths of this method are in its ability to visualize the placement-reach design problem and in its broadly applicable mathematical formulation well suited for computer implementation. Furthermore, because the ergonomic design problem is indeed an optimization process, the use of optimization techniques in this work lends itself to addressing other standing problems. The formulation and code are demonstrated using a number of examples.

Keywords: Ergonomic design; Placement; Reachability; Reach envelope; Optimization

1. Introduction

Ergonomic design of workspaces surrounding human limbs has been a long-standing problem. Consider the placement of human operators in an assembly line or seating a person at a control panel where tools and instruments must be reached. Human modeling and simulation programs have commercially appeared that support the ergonomic design process and allow for digital mannequins to be manipulated. The goal of this work is to increase the capability of such programs in order to automatically calculate the best location and orientation of the human with respect to predefined target points. The result will be a location of the human that will allow for the most comfortable reach!

*Corresponding author. Tel.: +001-319-335-5676; fax: 001-319-335-5669.
E-mail address: amalek@engineering.uiowa.edu (K. Abdel-Malek).

0169-8141/$ - see front matter
doi:10.1016/j.ergon.2004.05.001

We propose a general numerical approach for the design of an environment wherein a number of points to be reached (called target points) are specified and where a mathematical method is developed to position and orient the limb's origin (e.g., the torso if the arm is considered). Used iteratively, the method presents an effective mathematically based approach to ergonomic design. Because of its analytic nature, visualization of the limb's reach envelope and placement are readily made available to the designer and are well suited for computer implementation.

Thus far, the idea of introducing a mathematical model for ergonomic modeling of human motion was unforeseeable. For example, a method for the determination of ergonomic parameters that relate people to objects in space was proposed by Costa et al. (1997). The authors state that mathematical models of human movements are complex to define and hard to solve and suggest the use of Artificial intelligence in Neural Systems (ANS) as an approach to the problem. Indeed, collection of data for simulation of human movement has been done by many researchers (Ciungradi et al., 1998), but there has never been a fundamental approach for optimizing the placement of a human operator. Furthermore, the study of human motion has led designers to produce ergonomic-based workstations, by addressing work postures, work height; adjustable chairs; foot/hand use; gravity; momentum within normal work area (Konz, 1990), all in an experimental manner, which is costly and is difficult to use in a design scenario (i.e., difficult to implement optimization methods for design). The proposed work will provide a viable venue to address such issues.

The torso and upper extremities have been modeled as four-link systems consisting of trunk, upper arm, lower arm, and hand, being regarded as a redundant manipulator with a total of eight degrees of freedom (DOF) (Jung et al., 1992; Jung and Park, 1994; Jung and Kee, 1996). The authors stated that inverse kinematics were used for solving the system and that the joint range availability was used as a performance function in order to guarantee local optimality (Jung and Park, 1994). Inverse kinematics is an expression given to the mathematics used in calculating joint variables given the position and orientation of the end-link (e.g., hand). While inverse kinematics of an eight DOF system is not only difficult to obtain, but is also not reliable because of the many redundant solutions that may arise. Indeed, the concept of inverse kinematics in reachability analysis and ergonomic design should only be considered for non-redundant systems. Before defining the problem, we introduce terms that are necessary for this discussion.

1. *Specified point* ($\mathbf{s}_p$): a point embedded into the limb (e.g., the tip of a finger) whose motion will be tracked (Fig. 1a).
2. *Target points* ($\mathbf{p}_i$): are points defined in space and are to be touched by the specified point on the human limb as shown in Fig. 1a.

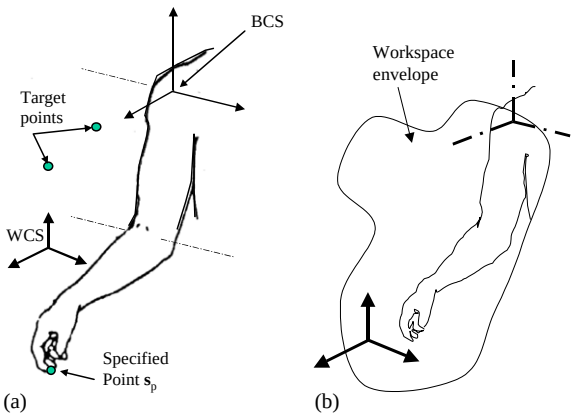

Fig. 1. (a) The point $\mathbf{s}_p$, BCS, WCS, and target points. (b) The workspace envelope of the arm.

3. *Base coordinate system* (BCS): is the first coordinate system in a series of consecutively numbered triads (Fig. 1a). The goal is to place the BCS such that the limb will satisfy the given constraints (e.g. reach all points, or maximize a given function).
4. *World coordinate system* (WCS): is a fixed invariant global coordinate system.
5. *Workspace envelope*: is an envelope that encloses the totality of points that can be touched by the specified point $\mathbf{s}_p$ on the limb [also called the *Reach Envelope* (Molenbroek, 1998)].
6. *Drive the workspace*: is an expression used to characterize impelling (causing a motion) of the workspace to minimize/maximize a cost function and will be used throughout this work to denote the repositioning and reorienting of the human.
7. *Cost function*: an objective function used in the optimization.

2. Problem definition

The reader must remember that this formulation is implemented in computer code and is intended for use by a designer to ergonomically place a human with respect to target points (e.g., handles, levers, gauges, etc.). Given a set of target points, a cost function, and a complete definition of an extremity (e.g., dimensions and ranges of motion of an arm), it is required to place the human with respect to these target points in such a way that the given cost function is optimized. This cost function characterizes human performance measures such as reachability, dexterity, stress, effort, discomfort, or potential energy. In this work, we will focus on reachability and stress at joints.

We present a mathematical formulation based on the following steps:

(1) Locate the target points $\mathbf{p}_i$ (e.g., instruments/devices/levers) at specific positions in 3D space (each target point is defined by a triplet-*xyz*).
(2) Identify the workspace of the limb. The workspace is characterized by a number of surface patches on the boundary envelope.
(3) Define a suitable cost function. Depending on the intended application, an appropriate cost function can be defined such as maximizing the reachability to all points, maximizing the dexterity at a target point, or minimizing the effort needed to move from one point to another.
(4) Numerically position and orient the workspace envelope to reach a configuration where all target points are inside the workspace while optimizing the given cost function. This step will guarantee that all target points (instruments/devices/levers) can be reached. The cost function is used here to drive (move, push, or impel) the workspace envelope.

In the following section, we will establish mathematical constraints whereby the ergonomic design problem will be formulated as a numerical optimization problem. Constraints that assure the inclusion of the target points inside the limb's workspace are necessary. The goal is to pose the problem in a manner that can be addressed using well-established mature optimization techniques but yet that does not need to compute the inverse kinematics of the limb. Inverse kinematics for limb models of high number of DOF are very difficult to achieve. The general algorithm for ergonomic design using the proposed cost functions is presented in Fig. 2, where $\mathbf{w}$ denotes the six generalized coordinates (explained in detail below) that will be used to track the location of the placement.

3. Delineating the envelope of the limb's workspace

In previous work applied to robotic manipulators (Abdel-Malek and Yeh, 1997), we have introduced a method for delineating surface patches that define the exact reach envelope of a kinematic chain in closed

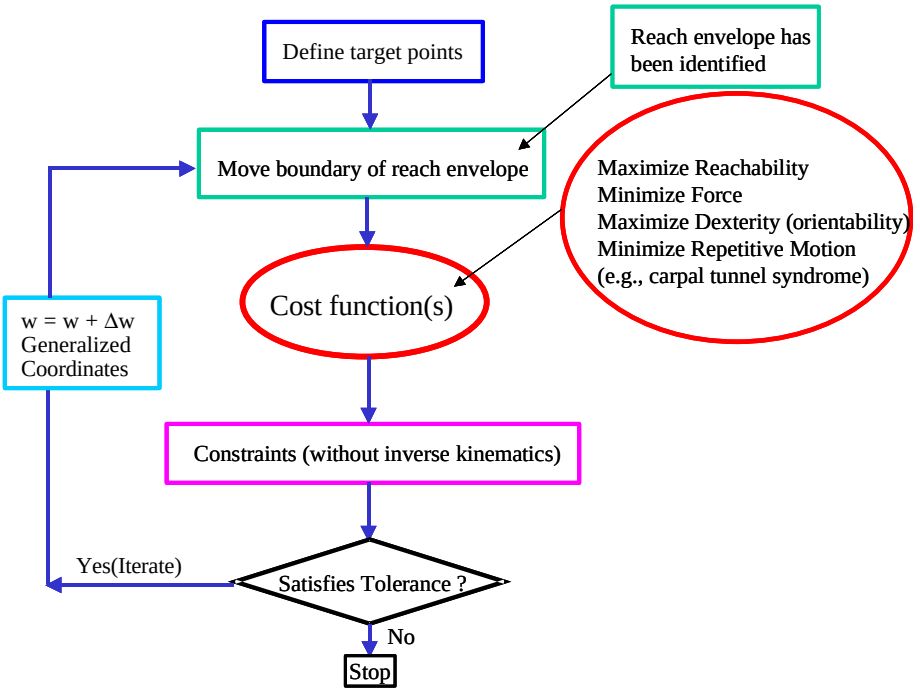

Fig. 2. Algorithm for ergonomic design.

form. In this section, we review this method, apply the methodology to human extremities, and define the needed surface patches.

Consider, for example, a specified point $\mathbf{s}_p$ on the tip of a finger as shown in Fig. 3. The position vector generated by this point with respect to the BCS for an arm represented by n-DOF is expressed by

$$\mathbf{\Phi}(\mathbf{q}) = [x(\mathbf{q}) \;\; y(\mathbf{q}) \;\; z(\mathbf{q})]^{\mathrm{T}}, \tag{1}$$

where $\mathbf{q} = [q_1, q_2, ..., q_n]^{\mathrm{T}} \in \mathbf{R}^n$ are the joint variables and $\mathbf{\Phi}(\mathbf{q})$ characterizes the vector set of all points that belong to the workspace (i.e., the volume touched by $\mathbf{s}_p$) and shown in Fig. 3.

In order to take into consideration the ranges of motion of each joint usually given in terms of an inequality constraint as

$$q_i^{\mathrm{L}} \leqslant q_i \leqslant q_i^{\mathrm{U}}, \tag{2}$$

we convert the joint ranges expressed by the inequalities of Eq. (2) to equalities, where the vector of joints variables is now a $\mathbf{q} = \mathbf{q}(\boldsymbol{\lambda})$, where $\boldsymbol{\lambda} = [\lambda_1, \ldots, \lambda_n]^{\mathrm{T}}$ are the new variables such that (see Appendix A for the parameterization)

$$\mathbf{\Phi} = \mathbf{\Phi}(\mathbf{q}(\boldsymbol{\lambda})). \tag{3}$$

This analysis was first demonstrated for the visualization of the workspace of robot manipulators (Abdel-Malek and Yeh, 1997; Abdel-Malek et al., 1999). Surfaces enveloping the workspace are analytically determined by studying the $(3 \times n)$ Jacobian matrix (from the German Mathematician Jacobi), which represents the differentiation of $\mathbf{\Phi}$ with respect to $\mathbf{q}$ as

$$\mathbf{\Phi}_{\mathbf{q}} = \left[\partial \Phi_i / \partial q_j\right], \quad i = 1, \ldots, 3 \text{ and } j = 1, \ldots, n, \tag{4}$$

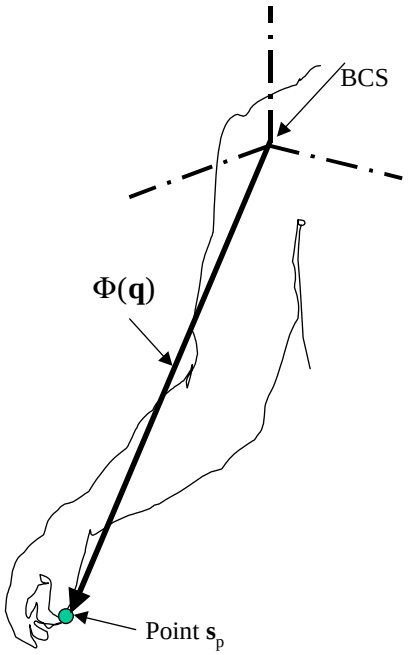

Fig. 3. Description of the $\mathbf{\Phi}(\mathbf{q})$ vector.

where Φ_i are the components of $\mathbf{\Phi}$ and q_j are the components of $\mathbf{q}$. An expression for the velocity *of the point* $\mathbf{s}_p$ *on the finger* is obtained by differentiating $\mathbf{\Phi}(\mathbf{q})$ with respect to time and using the chain rule as

$$\dot{\mathbf{\Phi}} = \mathbf{\Phi}_{\boldsymbol{q}} \boldsymbol{q}_{\boldsymbol{\lambda}} \dot{\boldsymbol{\lambda}}, \tag{5}$$

where the terminology $\mathbf{q}_{\boldsymbol{\lambda}} = \partial \mathbf{q}/\partial \boldsymbol{\lambda}$ and $\dot{\boldsymbol{\lambda}} = \partial \boldsymbol{\lambda}/\partial t$.

It can be shown (Abdel-Malek and Yeh, 1997; Abdel-Malek et al., 1997, 1999) that the limb's workspace boundary is delineated by studying the rank deficiency of $\mathbf{\Phi}_{\mathbf{q}} \mathbf{q}_{\boldsymbol{\lambda}}$. Three rank deficiency conditions were derived to delineate singular sets, denoted $\mathbf{s}^{(i)}$; $i = 1, \ldots, w$, where w is the number of singular sets. Substituting $\mathbf{p}^{(i)}$ into $\mathbf{\Phi}(\mathbf{q})$ yields a number of surfaces $\boldsymbol{\xi}^{(i)}(\mathbf{u}^{(i)})$, where $\mathbf{u}^{(i)}$ is the new vector of generalized coordinates such that

$$\boldsymbol{\xi}^{(i)}(\mathbf{u}^{(i)}) = \mathbf{\Phi}(\mathbf{u}^{(i)}, \mathbf{s}^{(i)}), \tag{6}$$

where $\mathbf{s}^{(i)}$ are obtained by solving a set of analytic functions called varieties (Lu 1978 and Spivak, 1968). Furthermore, surface patches in closed-form *on the boundary* of the envelope are a subset of Eq. (6) defined as $\boldsymbol{\xi}^{(i)}(\mathbf{u}^{(i)})$; $i = 1, \ldots, m$, where m is the number of patches enveloping the workspace as illustrated in Fig. 4b for the arm shown in Fig. 4a. Let $[\mathbf{x}\ \mathbf{y}\ \mathbf{z}]$ be the WCS and let $[\mathbf{x}_o\ \ \mathbf{y}_o\ \ \mathbf{z}_o]$ be the BCS associated with the shoulder (i.e., embedded in the torso) and that is initially coinciding with the WCS (Fig. 4a). Let there be m number of surface patches on the boundary as illustrated in Fig. 4b (i.e., we have a complete definition of the workspace) as

$$\boldsymbol{\eta} = \left\{ \boldsymbol{\xi}^{(i)}(\mathbf{u}^{(i)});\ i = 1, ..., m \text{ for } \mathbf{u}_{\mathrm{L}}^{(i)} \leqslant \mathbf{u}^{(i)} \leqslant \mathbf{u}_{\mathrm{U}}^{(i)} \right\}, \tag{7}$$

where $\mathbf{u}_{\mathrm{L}}^{(i)}$ and $\mathbf{u}_{\mathrm{U}}^{(i)}$ are the lower and upper limits, respectively, of the surface patch and $\boldsymbol{\eta}$ characterizes the envelope of the workspace.

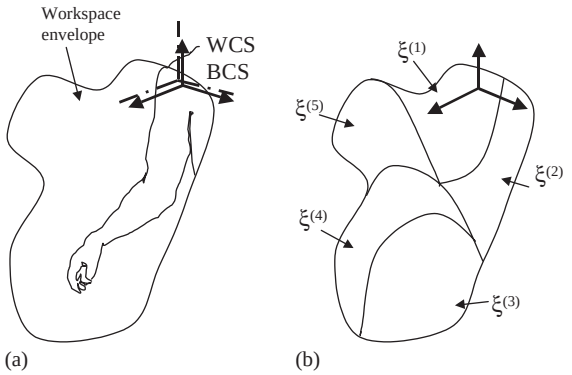

Fig. 4. (a) A human limb in the initial configuration with BCS and WCS coinciding, (b) the workspace envelope defined by the $\boldsymbol{\xi}^{(i)}(\mathbf{u}^{(i)})$ surface patches.

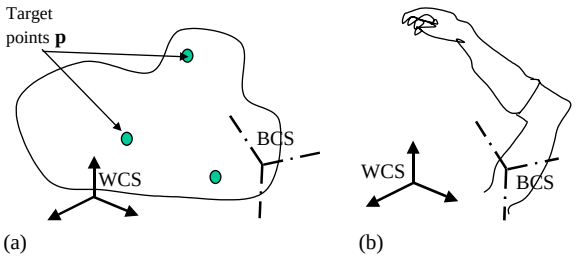

Fig. 5. (a) Workspace envelope after moving to include the target points, (b) the new configuration of the BCS.

4. Tracking the reach envelope

As both coordinate systems are initially coincident, effecting a translation and a rotation on the workspace of the limb will move the BCS triad $[\mathbf{x}_o \;\; \mathbf{y}_o \;\; \mathbf{z}_o]$ to a new location O_1 with coordinates $[x_w \;\; y_w \;\; z_w]$ and a new orientation defined by a set of Euler angles $(\alpha \;\; \beta \;\; \gamma)$ as shown in Fig. 5a and its placement of the BCS as shown in Fig. 5b.

We define the vector $\mathbf{w} = [x_w \;\; y_w \;\; z_w \;\; \alpha \;\; \beta \;\; \gamma]^{\mathrm{T}}$ as the vector of generalized coordinates that defines the translation and rotation of the BCS with respect to WCS and characterizes the configuration of the workspace. Motion of the workspace to a new configuration will be tracked using these six coordinates where the rotation matrix $\mathbf{R}$ and the position vector $\mathbf{v}$, are defined as

$$\mathbf{v} = [x_w \;\; y_w \;\; z_w]^{\mathrm{T}} \tag{8}$$

and

$$\mathbf{R}(\alpha,\beta,\gamma) = \begin{bmatrix} \cos\alpha\cos\beta & \cos\alpha\sin\beta\sin\gamma - \sin\alpha\cos\gamma & \cos\alpha\sin\beta\cos\gamma + \sin\alpha\sin\gamma \\ \sin\alpha\cos\beta & \sin\alpha\sin\beta\sin\gamma + \cos\alpha\cos\gamma & \sin\alpha\sin\beta\cos\gamma - \cos\alpha\sin\gamma \\ -\sin\beta & \cos\beta\sin\gamma & \cos\beta\cos\gamma \end{bmatrix}. \tag{9}$$

In order to track the motion of the envelope defined by surface patches $\boldsymbol{\xi}^{(i)}(\mathbf{u}^{(i)}), \quad i = 1, \ldots, m$, we multiply the surface patches by the rotation matrix and position vector as a function of $\mathbf{w}$.

$$\boldsymbol{\Psi}^{(i)}(\mathbf{w},\mathbf{u}) = \mathbf{R}(\alpha,\beta,\gamma)\cdot\boldsymbol{\xi}^{(i)}(\mathbf{u}) + \mathbf{v}(x_w, y_w, z_w). \tag{10}$$

The aim of this work is to determine the vector $\mathbf{w}$ that defines the new position and orientation of the BCS (therefore of the workspace envelope and consequently of the human) after moving to a new configuration thereby enclosing the specified target points, and driven by the cost function. The formulation that follows is developed to set forth the conditions for calculating a new configuration of the BCS via driving the workspace towards the target points.

5. Specifying the cost function

5.1. Reachability

Criteria for establishing whether a point is inside the workspace must be defined (i.e., is the point reachable?). In order to have a rigorous formulation, we develop a number of generalized constraints that are *not based on the inverse kinematics* of the arm. In order to track motion of the workspace envelope, the translated and rotated workspace is given by

$$\mathbf{\Gamma}(\mathbf{w},\mathbf{q}) = \mathbf{R}(\alpha,\beta,\gamma)\mathbf{\Phi}(\mathbf{q}) + \mathbf{v}(x_w, y_w, z_w). \tag{11}$$

Consider a number of target points $\mathbf{p}_i, \quad i = 1, ..., \ell$, each with coordinates $(x_P, y_P, z_P)_i$ in the space and a reach envelope $\boldsymbol{\eta}$ of a given human limb (note that not only a limb, but a torso or combination thereof can be considered). In order to insure that the target points will be located within the limb's workspace volume, we define a distance constraint such that the distance between the target points and the workspace is minimized as

$$\min\|\mathbf{p}^{(i)} - \mathbf{\Gamma}(\mathbf{w},\mathbf{q})\| = 0 \quad \text{for } i = 1, \ldots, \ell. \tag{12}$$

To ascertain that a target point $\mathbf{p}$ is inside the workspace, additional conditions are needed. The absolute value of the distance between a target point and the boundary should be greater than a specified value ε (depth inside the workspace). This is done to insure that the target points are reachable, i.e. inside the workspace. The distance between all target points $\mathbf{p}^{(j)}$ and all surface patches $\mathbf{\Psi}^{(i)}(\mathbf{u})$ should be greater than a specified minimum value such as

$$\|\mathbf{p}^{(j)} - \mathbf{\Psi}^{(i)}(\mathbf{u}^{(i)}, \mathbf{w})\| \geqslant \varepsilon_j \quad \text{where } j = 1, \ldots, \ell \text{ and } i = 1, \ldots, m, \tag{13}$$

where $\varepsilon_j > 0$ are specified constants and m is the number of surface patches. If a target point satisfies both conditions of Eqs. (12) and (13), then this point is internal to the workspace (i.e, can be reached). Those conditions are enough to guarantee that the point will be reached but do not provide a *driver* function (or force) to move the workspace.

Therefore, we must introduce an objective function (also called a cost function) that drives the motion of the reach envelope. This cost function can be defined by the designer. For example, if only reachability is of interest, this cost function is defined as the total sum of distances from the target points to the surface patches (we will use this concept in the examples below).

5.2. Torque on joints

$$\boldsymbol{\tau} = \mathbf{F}^{\mathrm{T}}\mathbf{J}(\mathbf{q}), \tag{14}$$

where $\boldsymbol{\tau}$ denotes the $(n \times 1)$ vector of joint torques and $\mathbf{F}^{\mathrm{T}}$ is the $(m \times 1)$ vector of end-effector forces, where m is the dimension of the operational space of interest, and where $\mathbf{J}$ is the Jacobian of the limb. Note that

the analysis of forces and torques on serial chains can be found in many references (Tsai 2000, Sciavicco and Siciliano, 1996).

5.3. Discomfort

We first define the neutral position of a given joint regardless of the motion as q_i^N. It is well known that a joint experiences a significant amount of stress as it is displaced from its most neutral position. Although different people have different neutral positions for the same joint, this approximate measure provides a viable and simple measure for quantitatively identifying stress. To quantify this displacement over all degrees of freedom, we sum the variation from the neutral position for all joints. Again, we use w as weight values for each joint to emphasize that some joints' stress is deemed higher than others.

$$S = \sum_{i=1}^{n} w_i \left| q_i^N - q_i \right|. \tag{15}$$

6. Optimizing the location and orientation of the operator

For ℓ target points and m surface patches, the problem is posed as a constrained optimization problem where the cost function is defined as a minimization of the distance between all target points and all surface patches

$$D(\mathbf{w}, \mathbf{u}) = \min \left[\sum_{i=1}^{m} \sum_{j=1}^{\ell} \| \boldsymbol{\Psi}^{(i)}(\mathbf{w}, \mathbf{u}^{(i)}) - \mathbf{p}^{(j)} \| \right] \tag{16}$$

subject to the constraints defined above and repeated as follows:

(1) Workspace envelope at least covering the target points (shortest distance between target points)

$$g_i \equiv \min \| \mathbf{p}^{(i)} - \boldsymbol{\Gamma}(\mathbf{q}, \mathbf{w}) \| \leqslant \beta \quad \text{for } i = 1, \ldots, \ell, \tag{17}$$

where β is a small positive number and subject to the inequality constraints on joint ranges as

$$q_k^{\mathrm{L}} \leqslant q_k \leqslant q_k^{\mathrm{U}} \quad \text{for } k = 1, \ldots, n. \tag{18}$$

(2) Embedding the target points inside the workspace volume (a minimum distance between target points and surface patches).

$$g_\kappa \equiv \| \mathbf{p}^{(j)} - \boldsymbol{\Psi}^{(i)}(\mathbf{u}, \mathbf{w}) \| \geqslant \varepsilon_j \quad \text{for } i = 1, \ldots, m \quad \text{and } j = 1, \ldots, \ell, \quad \kappa = 1, \ldots, (\ell \times m), \tag{19}$$

where ε_j is the depth of the target point inside the workspace volume. There are $\ell + (\ell \times m) + n$ total number of constraints.

The aim is to define a new configuration for the manipulator base such that all target points are included. As will be shown in this section, several sub-problems utilize optimization methods to obtain a solution, but the general problem will focus on obtaining a single configuration where all target points are reached. An iterative method for obtaining a solution to the above constrained optimization problem is implemented

(Arora, 1989). Before initiating the algorithm, several constraints are usually violated and others inactive. In order to obtain a viable configuration, we will initiate an iterative procedure, where for each iteration, two independent constrained optimization sub-problems Eqs. (17) and (19) are solved to obtain a new set of variables $\mathbf{w}$. The step value and direction are obtained using a commercial package (DOT, 1999) and used in this iterative procedure. (Note that any other efficient optimization algorithm could have been used).

7. Example 1: a 2-joint shoulder–elbow illustrative example

This example will be used to illustrate the formulation and to demonstrate the concept of a cost function to drive the workspace. Consider the simplified arm model on a planar surface (surface of a table), where only two joints are active as shown in Fig. 6. The arm is modeled as two revolute joints. The specified point $\mathbf{s}_p$ is on the tip of the thumb and there are two target points that need be reached at $\mathbf{p}_1 = (-35, 12)$ and $\mathbf{p}_2 = (-25, -8)$, i.e., $\ell = 2$. It is required to specify the placement of the human with respect to these points while maximizing reachability.

Coordinates of the specified point $\mathbf{s}_p$ located at the tip of the thumb can be written as

$$\mathbf{\Phi}(\mathbf{q}) = [-5\cos(q_1+q_2) - 10\sin q_1 - 10\sin(q_1+q_2)\ 10\cos q_1 + 10\cos(q_1+q_2) - 5\sin(q_1+q_2)]^{\mathrm{T}} \quad (20)$$

with joint ranges imposed as $-120^{\circ} \leqslant q_1 \leqslant 70^{\circ}$ and $0^{\circ} \leqslant q_2 \leqslant 120^{\circ}$, where the thumb is located at $\mathbf{s}_p = [5 \quad 5 \quad 0]^{\mathrm{T}}$ with respect to the third coordinate system. The Jacobian is calculated as

$$\boldsymbol{\xi}_q = \begin{bmatrix} -5(2\cos q_1 + 2\cos(q_1+q_2) - \sin(q_1+q_2)) & 5(-2\cos(q_1+q_2) + \sin(q_1+q_2)) \\ -5(2\cos(q_1+q_2) + 2(\sin q_1 + \sin(q_1+q_2)) & -5(\cos(q_1+q_2) + 2\sin(q_1+q_2)) \end{bmatrix} \quad (21)$$

and

$$\mathbf{q}_{\lambda} = \begin{bmatrix} -0.436\cos\lambda_1 & 0 \\ 0 & 1.658\cos\lambda_2 \end{bmatrix}. \quad (22)$$

Using the rank deficiency criteria, there are four curve segments shown in Fig. 7 (exact reach curves) and that are determined in closed form as:

$$\boldsymbol{\xi}^{(1)} = [-5\cos q_1 - 20\sin q_1 \quad 20\cos q_1 - 5\sin q_1]^{\mathrm{T}}$$
$$(\text{at } q_1 = q_1^{\mathrm{L}}) \text{ for } 120^{\circ} \leqslant q_1 \leqslant 70^{\circ}$$

$$\xi^{(2)} = [-8.66\cos q_1 + 5(0.5\cos q_1 + 0.866\sin q_1) - 5\sin q_1\ 5\cos q_1 + 5(-0.866\cos q_1 + 0.5\sin q_1) - 8.66\sin q_1]^{\mathrm{T}}$$
$$(\text{at } q_2 = 120^{\circ}) \text{ for } 120^{\circ} \leqslant q_1 \leqslant 70^{\circ}$$

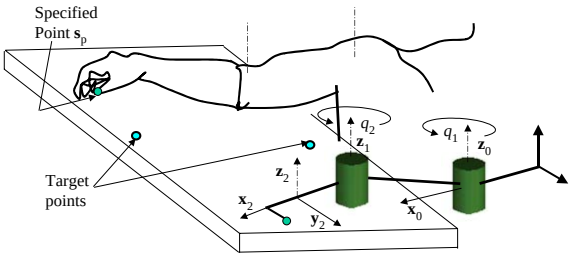

Fig. 6. Planar motion of the arm modeled as a two DOF system and target points specified.

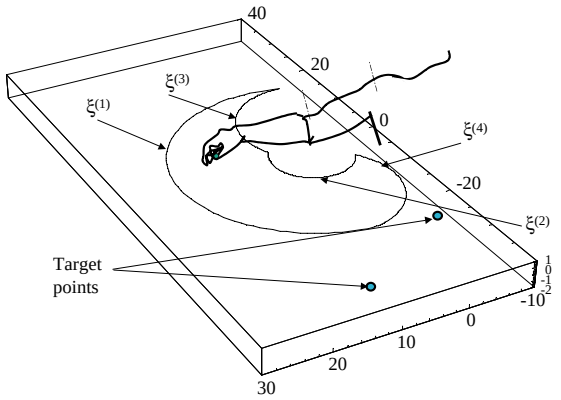

Fig. 7. The workspace envelope of the planar arm and the target.

Table 1
Initial and final configuration of the manipulator's base

Parameters	x_w	y_w	α
Initial	0.00	0.00	0.00°
Final	−19.3	6.8	134.5°

$$\boldsymbol{\xi}^{(3)} = \begin{bmatrix} 8.66 + 8.66\cos q_2 + 5(0.5\cos q_2 - 0.866\sin q_2) + 5\sin q_2 \\ -5 - 5\cos q_2 + 5(0.866\cos q_2 + 0.5\sin q_2) + 8.66\sin q_2 \end{bmatrix}$$
$$(\text{at } q_1 = q_1^{\mathrm{U}}) \text{ for } 0 \leqslant q_2 \leqslant 120^{\mathrm{o}}$$

$$\boldsymbol{\xi}^{(4)} = \begin{bmatrix} -9.39 - 9.39\cos q_2 + 5(-0.34\cos q_2 + 0.94\sin q_2) - 3.42\sin q_2 \\ 3.42 + 3.42\cos q_2 + 5(-0.94\cos q_2 - 0.34\sin q_2) - 9.39\sin q_2 \end{bmatrix}$$
$$(\text{at } q_1 = q_1^{\mathrm{U}}) \text{ for } 0 \leqslant q_2 \leqslant 120^{\mathrm{o}}.$$

Curves are shown in Fig. 7 and characterize the exact reach envelope of the 2-DOF arm.

We define the cost function in this simple case as the distance subtended from the target points to the curve segments $\boldsymbol{\xi}^{(i)}$. Implementing the numerical algorithm presented above such that the workspace envelope is driven towards the target points with the generalized variables $\mathbf{w} = [x_w\ y_w\ \alpha]^{\mathrm{T}}$, the initial and final configurations are presented in Table 1.

The initial and final configurations of the workspace envelope are shown in Fig. 8. The numerical results obtained from this algorithm are significant in many respects. They demonstrate that it is possible to rigorously define the reachability criteria and numerically design (or change) the layout to best obtain an ergonomic setup subject to a predefined cost function. This algorithm implemented in computer code is iteratively used to obtain designs based on visual and exact limb workspace analyses. Furthermore, researchers in other fields may elect to use different cost functions.

8. Example 2: upper extremity

Consider a model of the glenohumeral, elbow, and wrist joints shown in Fig. 9a and modeled as shown in Fig. 9b. The glenohumeral joint will be limited to 2DOF, the elbow to 1DOF, and the wrist to 2DOF.

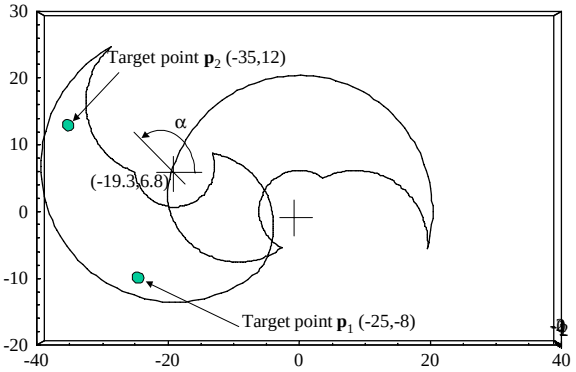

Fig. 8. Driving the workspace envelope to enclose the target points.

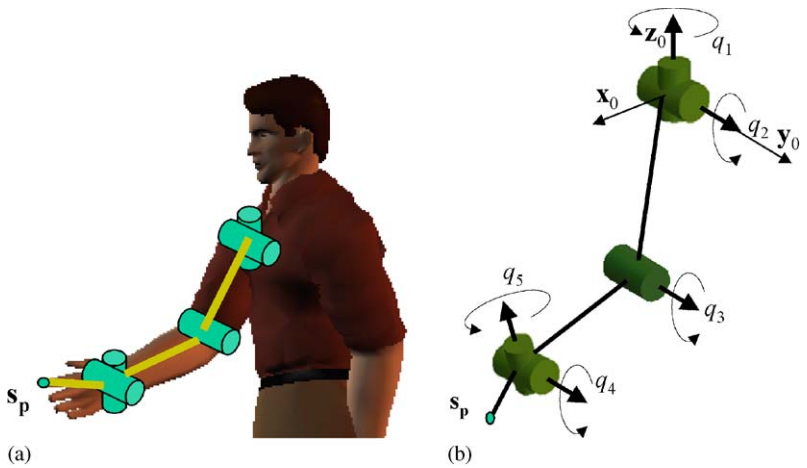

Fig. 9. (a) The specified point on the index finger, (b) the arm modeled as a 5-joint system.

Typical joint ranges are imposed as $-90^\circ \leqslant q_1 \leqslant 90^\circ$, $-110^\circ \leqslant q_2 \leqslant 120^\circ$, $0 \leqslant q_3 \leqslant 150^\circ$, $-20^\circ \leqslant q_4 \leqslant 40^\circ$, and $-70^\circ \leqslant q_5 \leqslant 80^\circ$.

A point on the end-effector is characterized by the position vector

$$\mathbf{\Phi}(\mathbf{q}) = \begin{bmatrix} 5(c_5 s_1 s_4 + c_1(-s_2(2s_3 + c_4 c_5 s_3 + c_3 s_5) + c_2(2 + 2c_3 + c_3 c_4 c_5 - s_3 s_5))) \\ 5(c_1 c_5 s_4 - s_1 s_2(2s_3 + c_4 c_5 s_3 + c_3 s_5) + c_2 s_1(2 + c_3(2 + c_4 c_5) - s_3 s_5)) \\ -5(c_2((2 + c_4 c_5)s_3 + c_3 s_5) + s_2(2 + c_3(2 + c_4 c_5) - s_3 s_5)) \end{bmatrix}, \tag{23}$$

where s_i denotes $\sin q_i$ and c_i denotes $\cos q_i$. Analysis of the Jacobian $\mathbf{\Phi}_{\mathbf{q}}\mathbf{q}_{\dot{\lambda}}$ yields the following singular sets:

Type I singularities

$$\mathbf{s}_1 = \{q_2 = \pi/2, q_3 = 0, q_5 = 0\},$$
$$\mathbf{s}_2 = \{q_2 = -\pi/2, q_3 = 0, q_5 = 0\},$$
$$\mathbf{s}_3 = \{q_3 = 0, q_4 = 0, q_5 = 0\}.$$

Type II singularities

(a) *Type II with one joint that has reached a limit*

$$\mathbf{s}_4 = \{q_2 = q_2^L, q_4 = 0, q_5 = 0\},$$
$$\mathbf{s}_5 = \{q_2 = q_2^U, q_4 = 0, q_5 = 0\},$$
$$\mathbf{s}_6 = \{q_3 = q_3^L, q_4 = 0, q_5 = 0\},$$
$$\mathbf{s}_7 = \{q_3 = q_3^U, q_4 = 0, q_5 = 0\}$$

(b) *Type II with two joints that have reached their limits* (listed in Appendix B)

Type III Singular sets

Additional 80 singular sets are due to rank deficiency 3 (i.e., at least three joints simultaneously at their limits). For example,

$$\mathbf{s}_{33} = \{q_1 = q_1^{\mathrm{L}}, q_2 = q_2^{\mathrm{L}}, q_3 = q_3^{\mathrm{L}}\},$$

$$\mathbf{s}_{34} = \{q_1 = q_1^{\mathrm{L}}, q_2 = q_2^{\mathrm{L}}, q_3 = q_3^{\mathrm{U}}\}.$$

In order to visualize these surfaces, we substitute the singular set into Eq. (23). Substituting other singularities into Eq. (23) yields equations of surfaces that are shown in Fig. 10(a–e).

The complete workspace envelope of the 5-DOF model of the arm is shown in Fig. 11.

The configuration of the BCS is described by the vector $\mathbf{w} = [x_w\ y_w\ z_w\ \alpha\ \beta\ \gamma]^{\mathrm{T}}$. Because the resulting workspace is indeed complex in nature with 112 surfaces, we introduce cross-sectional cuts through the reach envelope (the reader must note that this is only possible because of the closed form formulation). Consider, for example, the cross-section of an xy-plane through the workspace of the arm at $z=0$ (plan view) and the cross-section of an xz plane at $y=0$ (side and elevation views) as shown in Fig. 12(a) and (b).

Consider four target points located in space at known coordinates as illustrated in Fig. 13, where the person is to be placed into the environment. It is therefore required to move the workspace in such a way to maximize reachability (i.e., maximize the ability to reach all four points). The result of the algorithm is shown in Fig. 14, where the human has been relocated (placed) in the environment.

9. Example 3: lower extremity for minimum torque

Consider the lower extremity of a human modeled as four revolute joints shown in Fig. 15a, with the following joint constraints: $-90^\circ \leqslant q_4 \leqslant 90^\circ$, $-180^\circ \leqslant q_3 \leqslant 30^\circ$, $0^\circ \leqslant q_2 \leqslant 330^\circ$, and $0^{\mathrm{o}} \leqslant q_1 \leqslant 210^{\mathrm{o}}$. The workspace envelope of a point s_{p} (at the tip of the foot) with respect to the hip is shown in Fig. 15.

Consider a situation where it is required to design the interior of a vehicle such that the driver is seated in a way that would allow his/her foot to exert a given force on a number of pedals yet while minimizing stress on each joint. The designer will use a human modeling and simulation code to perform the analysis and finally select a design.

The position vector function characterizing the workspace is given by

$$\mathbf{\Phi}(\mathbf{q}) = \begin{bmatrix} \cos q_1(10 + 5\cos q_2 + 3\cos(q_2 + q_3) + \cos(q_2 + q_3 + q_4)) \\ \sin q_1(10 + 5\cos q_2 + 3\cos(q_2 + q_3) + \cos(q_2 + q_3 + q_4)) \\ 7 + 5\sin q_2 + 3\sin(q_2 + q_3) + \sin(q_2 + q_3 + q_4) \end{bmatrix}. \tag{24}$$

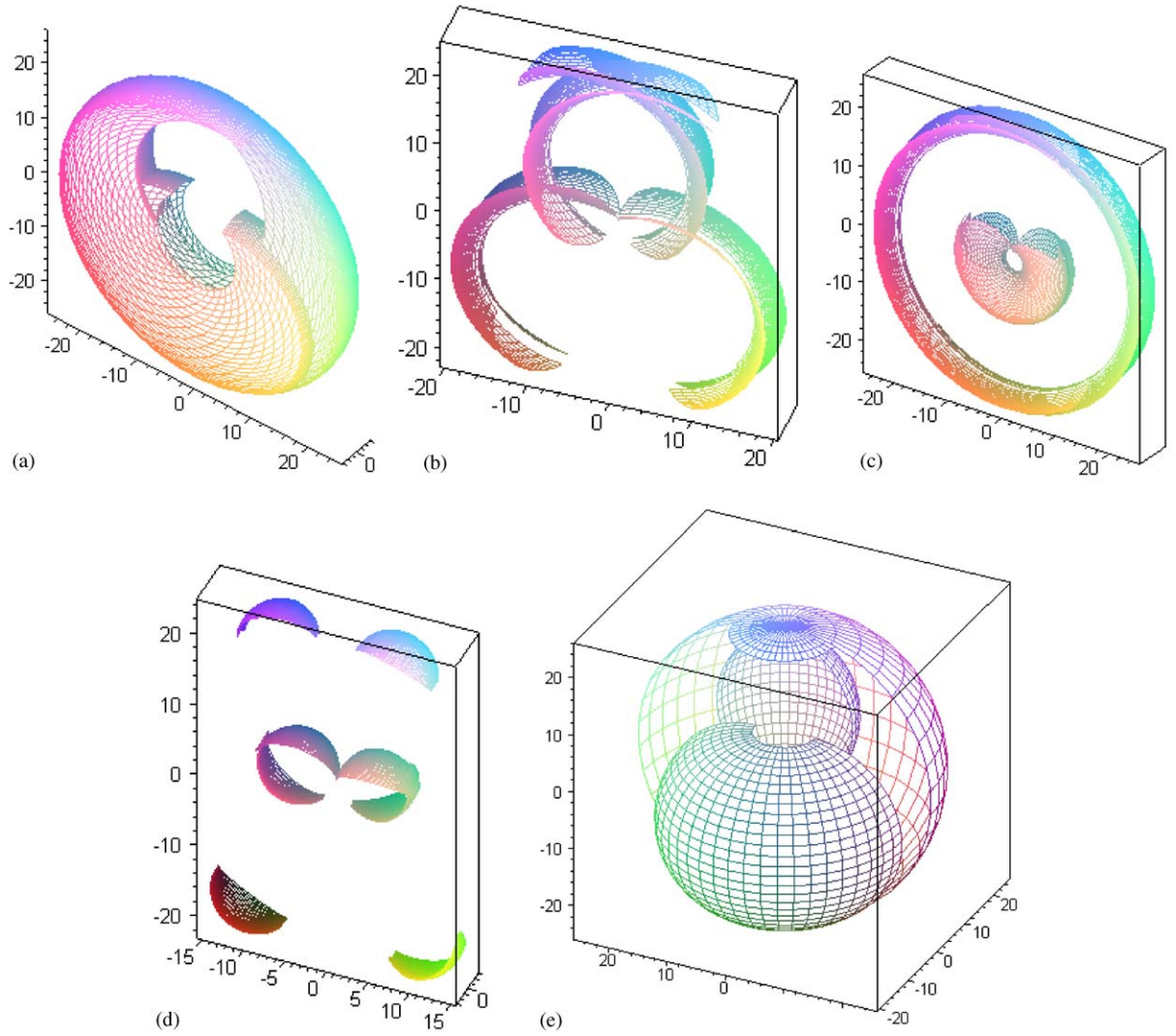

Fig. 10. Type II singularities due to (a) $\mathbf{s}_{8-16}$, (b) $\mathbf{s}_{40-48}$, (c) $\mathbf{s}_{64-72}$, (d) $\mathbf{s}_{32-80}$, (e) $\mathbf{s}_{4-8}$.

Jacobian rank-deficiency conditions applied to $\mathbf{\Phi_q q_\lambda}$ yield a number of singular sets, and surface patches on the boundary are delineated and characterized by the following sets:

$$\mathbf{x}^{(17b)}(q_1, q_3); 0^o \leqslant q_1 \leqslant 210^o \text{ and } -\pi \leqslant q_3 \leqslant -175^o,$$

$$\mathbf{x}^{(9)}(q_1, q_4); 0^o \leqslant q_1 \leqslant 210^o \text{ and } -17^o \leqslant q_4 \leqslant 0^o,$$

$$\mathbf{x}^{(15)}(q_1, q_2); 0^o \leqslant q_1 \leqslant 210^o \text{ and } 0^o \leqslant q_2 \leqslant 330^o,$$

$$\mathbf{x}^{(19)}(q_1, q_2); 0^o \leqslant q_1 \leqslant 210^o \text{ and } 0 \leqslant q_2 \leqslant 330^o,$$

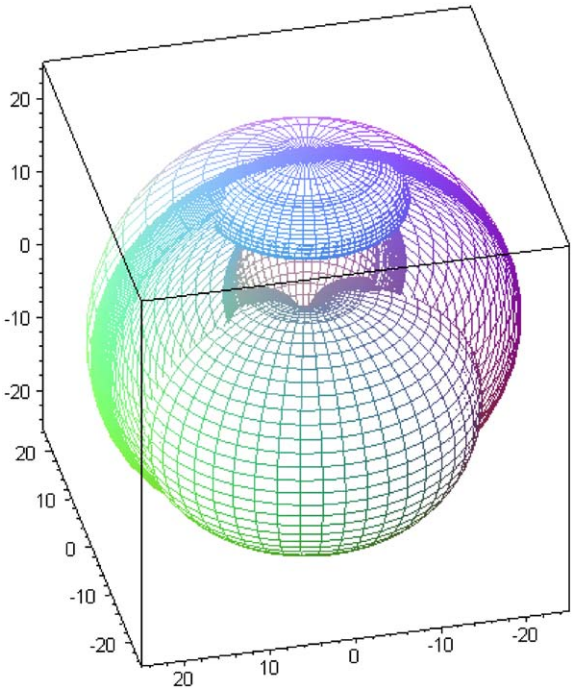

Fig. 11. The reach envelope of the 5-DOF arm model.

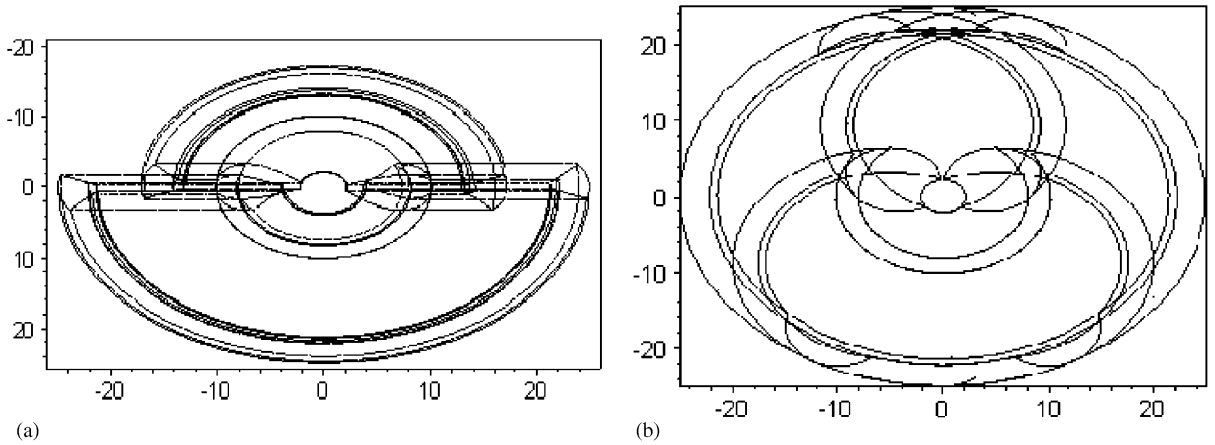

(a) (b)

Fig. 12. (a) An *xy* cross-sectional plane through the workspace of the arm, (b) an *xz* cross-sectional plane through the workspace of the arm.

$$\mathbf{x}^{(17c)}(q_1, q_3); 0^o \leqslant q_1 \leqslant 210^o \text{ and } -34^o \leqslant q_3 \leqslant 7^o,$$

$$\mathbf{x}^{(18)}(q_1, q_3); 0^o \leqslant q_1 \leqslant 210^o \text{ and } 0^o \leqslant q_3 \leqslant 30^o,$$

$$\mathbf{x}^{(10)}(q_1, q_4); 0^o \leqslant q_1 \leqslant 210^o \text{ and } -20^o \leqslant q_4 \leqslant 20^o,$$

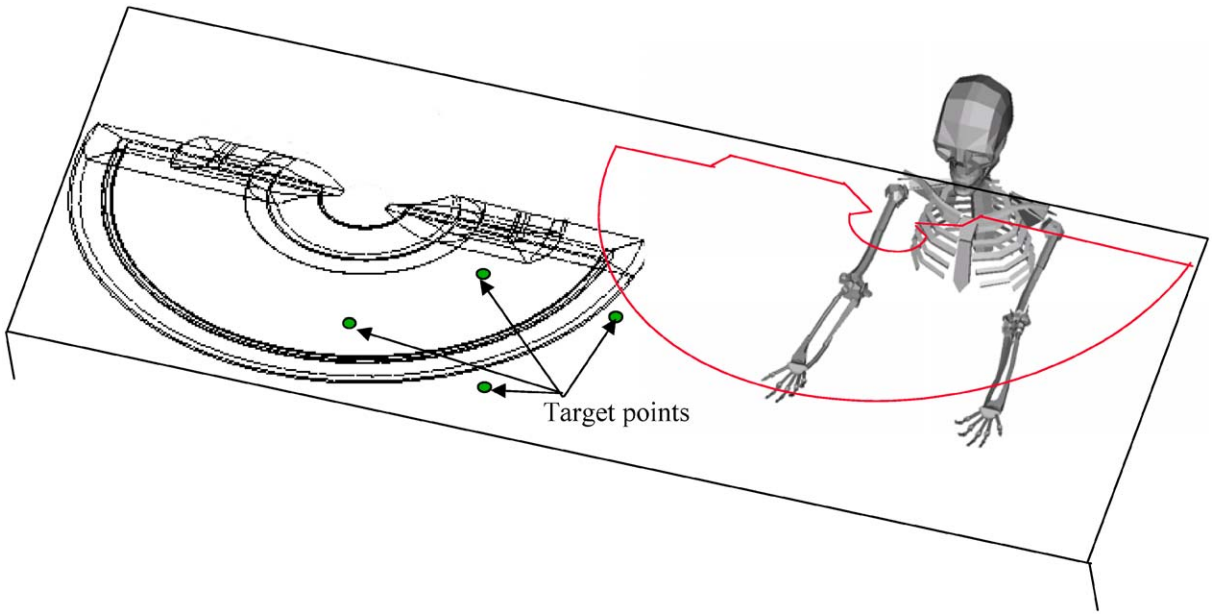

Fig. 13. Moving the workspace towards reaching all target points with minimum distance.

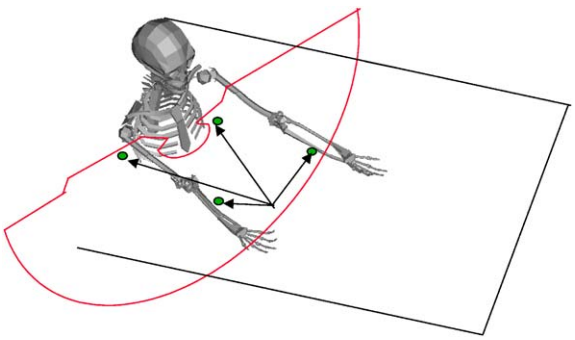

Fig. 14. The new configuration of the seating.

$\mathbf{x}^{(5)}(q_1, q_2); 0^o \leqslant q_1 \leqslant 210^o$ and $276^o \leqslant q_2 \leqslant 283^o$,

$\mathbf{x}^{(17a)}(q_1, q_3); 0^o \leqslant q_1 \leqslant 210^o$ and $-154^o \leqslant q_3 \leqslant -70^o$,

$\mathbf{x}^{(8)}(q_1, q_2); 0^o \leqslant q_1 \leqslant 210^o$ and $293^o \leqslant q_2 \leqslant 312^o$, and

$\mathbf{x}^{(11)}(q_1, q_3); 0^o \leqslant q_1 \leqslant 210^o$ and $-142^o \leqslant q_3 \leqslant -30^o$.

Substituting these sets into Eq. (24) yields parametric equations of singular surfaces shown in Fig. 16 (a cross-section of the workspace is shown).

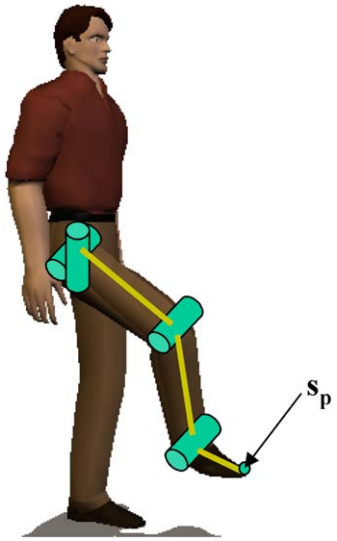

Fig. 15. Modeling of the lower extremity as a 4-revolute kinematic chain.

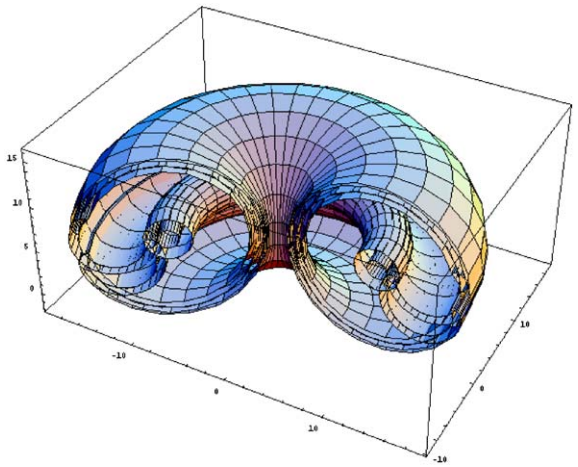

Fig. 16. Workspace envelope of the lower extremity.

In order to perform the iterative algorithm while minimizing torque on joints, it is necessary to develop an analytic expression for the Jacobian of the 4-revolute model relating the linear and angular velocity to joint rates as

$$\boldsymbol{J}^{4\mathrm{dof}}(\boldsymbol{q}) = \begin{bmatrix} J_{11} & J_{12} & J_{13} & J_{14} \\ J_{21} & J_{22} & J_{23} & J_{24} \\ J_{31} & J_{32} & J_{33} & J_{34} \\ J_{41} & J_{42} & J_{43} & J_{44} \\ J_{51} & J_{52} & J_{53} & J_{54} \\ J_{61} & J_{62} & J_{63} & J_{64} \end{bmatrix}_{6\times 4},$$

where

$$
\begin{aligned}
J_{14} &= -\cos(q_1)\sin(q_2+q_3+q_4),\\
J_{24} &= -\sin(q_1)\sin(q_2+q_3+q_4),\\
J_{34} &= \cos(q_2+q_3+q_4),\\
J_{13} &= -\cos(q_1)\,(3.0\sin(q_2+q_3)\\
&\quad +\sin(q_2+q_3+q_4)),\\
J_{23} &= -\sin(q_1)\,(3.0\sin(q_2+q_3)\\
&\quad +\sin(q_2+q_3+q_4)),\\
J_{33} &= 3.0\cos(q_2+q_3)+\cos(q_2+q_3+q_4),\\
J_{12} &= -\cos(q_1)\,(5.0\sin(q_2)+3.0\sin(q_2+q_3)\\
&\quad +\sin(q_2+q_3+q_4)),\\
J_{22} &= -\sin(q_1)\,(5.0\sin(q_2)+3.0\sin(q_2+q_3)\\
&\quad +\sin(q_2+q_3+q_4)),\\
J_{32} &= 5.0\cos(q_2)+3.0\cos(q_2+q_3)\\
&\quad +\cos(q_2+q_3+q_4),\\
J_{11} &= -\sin(q_1)\,(10.0-\sin(q_2)\,((3+\cos(q_4))^{*}\\
&\quad \times\sin(q_3)+\cos(q_3)\sin(q_4))+\cos(q_2)^{*}\\
&\quad \times(5+\cos(q_3)\,(3+\cos(q_4))-\sin(q_3)\sin(q_4))),\\
J_{21} &= \cos(q1)\,(10.0+5.0\cos(q2)\\
&\quad +3.0\cos(q2+q3)+\cos(q2+q3+q4)),\\
J_{31} &= 0.0,\\
J_{41} &= 0.0,\\
J_{42} &= \sin(q_1),\\
J_{43} &= \sin(q_1),\\
J_{44} &= \sin(q_1),\\
J_{51} &= 0.0,\\
J_{52} &= -\cos(q_1),\\
J_{53} &= -\cos(q_1),\\
J_{54} &= -\cos(q_1),\\
J_{61} &= 1.0,\\
J_{62} &= 0.0,\\
J_{63} &= 0.0,\\
J_{64} &= 0.0.
\end{aligned}
$$

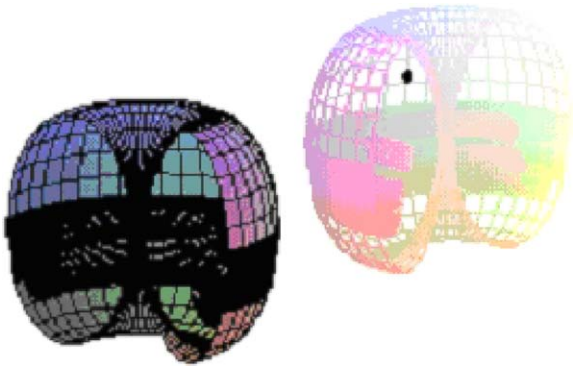

Fig. 17. The initial and final position of the workspace.

For the given target point at **P**(30,30,10) and a given force vector at the foot of **F**(1, 1, 1, 1, 1, 1), we implement the proposed method. The iterative optimization algorithm yields the coordinates of the hip at (22.6, 20.6, 1.25) with the following orientation angles (2.76, −3.14, −3.14) (units in radians). The corresponding posture for minimum torque on all joints is when

$$q_1 = 2.3284,$$
$$q_2 = 2.2723,$$
$$q_3 = 0.3451,$$
$$q_4 = 1.0154.$$

The initial and final positions of the workspace envelope are shown in Fig. 17.

10. Conclusions

Ergonomic design has depended upon trial and error and vastly on empirical data, whereby experience and rules of thumb are used. Nevertheless, it is widely understood that ergonomic design is indeed an optimization problem with many parameters. This paper presents a mathematical approach to ergonomic design using well-established methods in optimization and workspace analysis.

It was shown that the workspace envelope of any human limb is rigorously identified using criteria developed from the row rank deficiency of the Jacobian, while taking into consideration ranges of motion. These ranges are imposed in terms of inequality constraints that are converted into equality constraints. The boundary surfaces/curves are determined in closed form and readily visualized. Boundary surface patches (or curve segments) were delineated. Placement of a person in the environment is performed by driving the workspace towards the target points using the cost function and subject to a set of constraints. The result is an ability to visualize the limb's workspace envelope in 3D and to mathematically explore operations that can be conducted on this workspace.

Because of the closed-form nature of these surfaces, it was shown that an ergonomic design is achieved based on a cost function and constraints defined by the user. For example, if the objective is to have the arm reach all points in the workspace, then the distance function to target points can be used. If the goal is to place the human such that he/she can reach a number of points while minimizing stress on each joint, a different cost function is imposed. The result is a placement of the workspace envelope (and hence the human) such that the cost function is optimized.

The motivation for such work stems from a need for accurately designing furniture, workstations, assembly lines, vehicle interiors, and general ergonomic workspaces. Whether for the design of control rooms, the placement of instrumentation and gauges, or for the design of furniture, this method will yield accurate mathematically-based results.

The potential for this work to play a key role in other fields is relevant. Future implementation of this work is aimed at designing the workspace to minimize repetitive motions that may over time lead to injuries, and to place humans while minimizing low back pain. This group is currently developing analytic models of such cost functions. The formulation developed herein was illustrated through examples of the upper and lower extremities with various cost functions.

Appendix A. Parameterization

A convenient parameterization of constraints imposed on $\mathbf{q}$ was presented such that joint inequality constraints $q_i^{\mathrm{L}} \leqslant q_i \leqslant q_i^{\mathrm{U}}$ are given by

$$\mathbf{q}(\boldsymbol{\lambda}) = (\mathbf{q}^{\mathrm{U}} + \mathbf{q}^{\mathrm{L}})/2 + [(\mathbf{q}^{\mathrm{U}} - \mathbf{q}^{\mathrm{L}})/2]\sin\boldsymbol{\lambda}, \tag{A.1}$$

where $\mathbf{q}^{\mathrm{U}} = [q_1^{\mathrm{U}}, \cdots, q_n^{\mathrm{U}}]^{\mathrm{T}}$ and $\mathbf{q}^{\mathrm{L}} = [q_1^{\mathrm{L}}, \cdots, q_1^{\mathrm{L}}]^{\mathrm{T}}$ are the upper and lower joint limits, respectively, and $\boldsymbol{\lambda} = [\lambda_1, \cdots, \lambda_n]^{\mathrm{T}}$ are the new variables that have been introduced by adding as many equations as the number of variables without reducing the dimensionality of the problem ($\boldsymbol{\lambda}$ are usually called slack variables in the field of optimization).

Appendix B. Type II singular sets

$$\mathbf{s}_8 = \{q_1 = q_1^{\mathrm{L}}, q_2 = q_2^{\mathrm{U}}, q_5 = 0\},$$
$$\mathbf{s}_9 = \{q_1 = q_1^{\mathrm{U}}, q_2 = q_2^{\mathrm{L}}, q_5 = 0\},$$

$$\mathbf{s}_{10} = \{q_1 = q_1^{\mathrm{U}}, q_2 = q_2^{\mathrm{U}}, q_5 = 0\},$$
$$\mathbf{s}_{11} = \{q_1 = q_1^{\mathrm{L}}, q_3 = q_3^{\mathrm{L}}, q_5 = 0\},$$
$$\mathbf{s}_{12} = \{q_1 = q_1^{\mathrm{U}}, q_3 = q_3^{\mathrm{L}}, q_5 = 0\},$$

$$\mathbf{s}_{13} = \{q_1 = q_1^{\mathrm{L}}, q_4 = q_4^{\mathrm{L}}, q_5 = 0\},$$
$$\mathbf{s}_{14} = \{q_1 = q_1^{\mathrm{L}}, q_4 = q_4^{\mathrm{U}}, q_5 = 0\},$$
$$\mathbf{s}_{15} = \{q_1 = q_1^{\mathrm{U}}, q_4 = q_4^{\mathrm{L}}, q_5 = 0\},$$

$$\mathbf{s}_{16} = \{q_1 = q_1^{\mathrm{U}}, q_4 = q_4^{\mathrm{U}}, q_5 = 0\},$$
$$\mathbf{s}_{17} = \{q_2 = q_2^{\mathrm{L}}, q_3 = q_3^{\mathrm{L}}, q_4 = 0\},$$
$$\mathbf{s}_{18} = \{q_2 = q_2^{\mathrm{L}}, q_3 = q_3^{\mathrm{U}}, q_4 = 0\},$$

$$\mathbf{s}_{19} = \{q_2 = q_2^{\mathrm{U}}, q_3 = q_3^{\mathrm{L}}, q_4 = 0\},$$
$$\mathbf{s}_{20} = \{q_2 = q_2^{\mathrm{U}}, q_3 = q_3^{\mathrm{U}}, q_4 = 0\},$$
$$\mathbf{s}_{21} = \{q_2 = q_2^{\mathrm{L}}, q_4 = q_4^{\mathrm{L}}, q_5 = 0\},$$

$$\mathbf{s}_{22} = \{q_2 = q_2^{\mathrm{L}}, q_4 = q_4^{\mathrm{U}}, q_5 = 0\},$$
$$\mathbf{s}_{23} = \{q_2 = q_2^{\mathrm{U}}, q_4 = q_4^{\mathrm{L}}, q_5 = 0\},$$
$$\mathbf{s}_{24} = \{q_2 = q_2^{\mathrm{U}}, q_4 = q_4^{\mathrm{U}}, q_5 = 0\},$$
$$\mathbf{s}_{25} = \{q_2 = q_2^{\mathrm{L}}, q_4 = 0, q_5 = q_5^{\mathrm{L}}\},$$
$$\mathbf{s}_{26} = \{q_2 = q_2^{\mathrm{L}}, q_4 = 0, q_5 = q_5^{\mathrm{U}}\},$$
$$\mathbf{s}_{27} = \{q_2 = q_2^{\mathrm{U}}, q_4 = 0, q_5 = q_5^{\mathrm{U}}\},$$
$$\mathbf{s}_{28} = \{q_3 = q_3^{\mathrm{L}}, q_4 = q_4^{\mathrm{L}}, q_5 = 0\},$$
$$\mathbf{s}_{29} = \{q_3 = q_3^{\mathrm{L}}, q_4 = q_4^{\mathrm{U}}, q_5 = 0\},$$
$$\mathbf{s}_{30} = \{q_3 = q_3^{\mathrm{L}}, q_5 = q_5^{\mathrm{L}}, q_4 = 0\},$$
$$\mathbf{s}_{31} = \{q_3 = q_3^{\mathrm{L}}, q_5 = q_5^{\mathrm{U}}, q_4 = 0\}, \text{ and}$$
$$\mathbf{s}_{32} = \{q_1 = q_1^{\mathrm{L}}, q_2 = q_2^{\mathrm{L}}, q_5 = 0\}.$$

References

Abdel-Malek, K., Yeh, H.J., 1997. Analytical boundary of the workspace for general three degree-of-freedom mechanisms. International Journal of Robotics Research 16 (2), 198–213.

Abdel-Malek, K., Adkins, F., Yeh, H.J., Haug, E.J., 1997. On the determination of boundaries to manipulator workspaces. Robotics and Computer-Integrated Manufacturing 13 (1), 63–72.

Abdel-Malek, K., Yeh, H.-J., Khairallah, N., 1999. Workspace, void, and volume determination of the general 5DOF manipulator. Mechanics of Structures and Machines 27 (1), 91–117.

Arora, J.S., 1989. Introduction to Optimum Design. McGraw-Hill, New York.

Ciungradi, B., Costa, M., Pasero, E., Macchiarulo, L., 1998. Recurrent network for data driven human movement generation. Proceedings of the 1998 IEEE International Joint Conference on Neural Networks. Part 1 (of 3), May 4–9, 1998 Vol. 1, Anchorage, AK, pp. 216–220.

Costa, M., Crispino, P., Hanomolo, A., Pasero, E., Artificial neural networks and the simulation of human movements in CAD environments. Proceedings of the 1997 IEEE International Conference on Neural Networks. Part 3 (of 4), June 9–12, 1997, Vol. 3, Houston, TX, pp. 1781–1784.

DOT 1999. Users Manual, VR&D, http://www.vrand.com

Jung, E.S., Kee, D., 1996. Man–machine interface model with improved visibility and reach functions. Computers and Industrial Engineering 30 (3), 475–486.

Jung, E.S., Kee, D., Chung, M.K., 1992. Reach posture prediction of upper limb for ergonomic workspace evaluation. Proceedings of the 36th Annual Meeting of the Human Factors Society, Part 1 (of 2) October 12–16 1992, Vol. 1, Atlanta, GA, pp. 702–706.

Jung, E.S., Park, S., 1994. Prediction of human reach posture using a neural network for ergonomic man models. Proceedings of the 16th Annual Conference on Computers and Industrial Engineering, Vol. 27, 1–4, September 1994, Ashikaga, Japan, pp. 369–372.

Konz, S., 1990. Workstation organization and design. International Journal of Industrial Ergonomics 6 (2), 175–193.

Molenbroek, J.F.M., 1998. Reach envelopes of older adults. Proceedings of the 1998 42nd Annual Meeting 'Human Factors and Ergonomics Society', October 5–9, 1998 Vol. 1. Chicago, IL, pp. 166–170.

Sciavicco, L., Siciliano, B., 1996. Modeling and Control of Robot Manipulators. McGraw Hill, New York.

Tsai, L.W., 2000. Robot Analysis: the Mechanics of Serial and Parallel Manipulators. Wiley, New York.